Eur. Phys. J. D **31**, 365–373 (2004)
DOI: 10.1140/epjd/e2004-00130-3

THE EUROPEAN PHYSICAL JOURNAL D

Slow ammonia molecules in an electrostatic quadrupole guide

T. Junglen, T. Rieger, S.A. Rangwala, P.W.H. Pinkse[a], and G. Rempe

Max-Planck-Institut für Quantenoptik, Hans-Kopfermann-Str. 1, 85748 Garching, Germany

Received 1st July 2004
Published online 28 September 2004 –

Abstract. An electrostatic quadrupole is used to filter slow dipolar ND_3 molecules from an effusive source and to guide them into ultrahigh vacuum. The molecules in the electrostatic quadrupole experience a Stark interaction which allows filtering of small velocities in the linear and bent sections of the quadrupole. With this technique we demonstrate a flux of $\approx 10^{10}$/s with a longitudinal temperature of a few K. The technique and the set-up are discussed in detail, and the guided gas as well as the output beam are characterized. Improvements in the set-up are highlighted, as for instance cooling of the effusive source to below 150 K.

PACS. 33.55.Be Zeeman and Stark effects – 39.10.+j Atomic and molecular beam sources and techniques

1 Introduction

At present, a growing interest in cold molecules motivates scientists in many fields of physics and chemistry to produce and control such samples. Cold molecules seem to be ideal test objects for high precision experiments and their availability promises, among other things, to extend the search for the electric dipole moment of the electron [1]. Molecules were recently used in matter wave interferometry experiments [2] which allow precise measurements of fundamental constants. Such experiments will benefit from the extended interaction times in cold molecular samples. In the field of cold chemistry the lower energy and the longer duration of collisions reveal new effects [3] and provide a deeper insight into chemical reactions. Demonstrated techniques to produce such samples are buffer-gas cooling [4], deceleration of molecules in time-varying electric fields [5–7], filtering slow molecules from an effusive source [8], and photoassociation of laser-cooled atoms [9–14]. Moreover, atomic physicists were recently able to observe the formation of molecules from ultracold atoms using Feshbach resonances [15–22]. Furthermore there exist several methods based on mechanical means [23] and, recently, molecules at subkelvin temperatures were obtained by collisions in a crossed molecular beam apparatus [24].

The method which we introduced in [8] exploits the fact that large quantities of slow molecules are present in any thermal gas even at room temperature and it is enough to filter them out efficiently. Let us consider molecules as slow if they can be trapped with electric, magnetic or electromagnetic fields. A practical upper limit of neutral particle trap depths is in the order of a kelvin, which is most easily achieved using electric fields. If this value is translated into a light polar molecule like ND_3 we see that it corresponds to velocities of ≈35 m/s. From the Maxwell-Boltzmann distribution at $T = 300$ K, we derive that the fraction of particles with a velocity below the cutoff velocity $v_0 = 35$ m/s is $\int_0^{35} 4\pi^{-1/2}\alpha^{-3}v^2 \exp[-v^2/\alpha^2]dv \approx 1\times10^{-4}$ in each volume element. The most probable velocity in the gas, $\alpha = \sqrt{2k_BT/m}$, where k_B is the Boltzmann constant and m the molecular mass, can be calculated to be $\alpha = 500$ m/s. Although being a small fraction, for a gas at standard pressure and temperature this results in a density of $\approx 10^{15}$ cm^{-3}. This small fraction but large number is the core motivation for our technique allowing efficient filtering of slow molecules from a gas reservoir even at room temperature.

The idea is sketched in Figure 1. It is based on the same filter *ansatz* exploited in an experiment using permanent magnets to filter out slow Li atoms from an oven [25]. We use an electrostatic quadrupole to filter the slow molecules from an effusive source. For the filtering process the interaction of polar molecules with electric fields is exploited. Molecules whose time averaged dipole moments are oriented antiparallel (parallel) to the external electric field minimize their internal energy in weak (strong) field regions and they are called low-field seekers [lfs] (high-field seekers [hfs]). The gas is injected at the electric-field minimum of the quadrupole. For the injected lfs molecules whose transverse kinetic energy is smaller than the Stark energy shift, transverse trapping results, while the rest escapes. Longitudinal velocity filtering in the bent section of the guide results from centripetal action keeping only the slowest molecules whereas longitudinally fast molecules escape. As the background pressure is comparatively high in the injection region, the slow molecules are guided

[a] e-mail: Pepijn.Pinkse@mpq.mpg.de

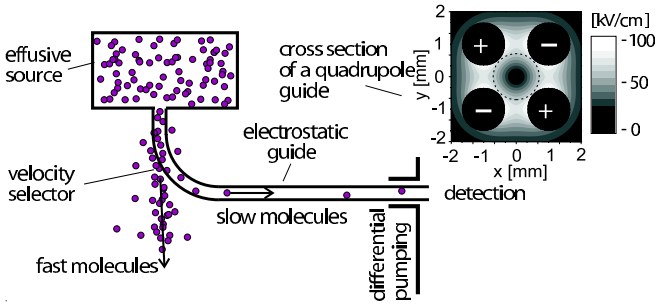

Fig. 1. Sketch of how to filter slow polar molecules from a thermal gas. Molecules from an effusive source are injected into a bent electrostatic quadrupole with a free inner radius r indicated by the dashed circle. Only transversely slow molecules which cannot overcome the Stark potential barrier are kept within the guide, whereas longitudinal velocity selection is provided by the bend. The fast molecules are pumped away and the slow molecules are guided into a separate ultrahigh-vacuum chamber.

through differential pumping stages into a better vacuum to reduce losses caused by background collisions.

This technique allows "on spot" delivery of slow molecules in a separate UHV chamber for further investigation without disturbing influences of the inlet beam. Compared to the set-up in [8] the new set-up described here uses two bent sections and two differential pumping stages in order to reach a better vacuum in the detection chamber. Furthermore, the quadrupole geometry has been changed to a configuration where the electrode distance now equals the rod radius. The new geometry provides a larger open guide cross-section which leads to a higher gas throughput as well as better mechanical stability. Another improvement is a cooling stage which enables precooling of the injected gas.

In this paper we characterize the new source: first a detailed calculation of the expected guidable flux of ND_3 at different temperatures is performed. Then we show experimental data where we measure the flux of cold molecules depending on the parameters: electrode voltage, inlet pressure and inlet temperature. The velocity distribution of the guided molecules is determined by a time-of-flight measurement and the exit beam angle distribution is also presented. Finally, the influence of a buffer gas admixture on the flux and the velocity distribution will be analysed and we close with an outlook on possible future extensions and improvements.

2 The Stark filter

Our molecules originate from an effusive source with a small exit channel through which the gas escapes from the high pressure side to the low pressure side. The molecules are injected directly into the guide. Therefore, it is essential that the source is maintained in the molecular flow regime, which means that the pressure at the exit channel or "nozzle" has to be reduced so far that the mean-free path exceeds the exit channel dimensions. If these conditions are ignored, the molecules will collide with each other when leaving the exit channel and the few slow molecules will be promoted to higher velocities by collisions with fast ones, effectively removing the lowest velocities in the velocity distribution of the effusing gas.

For a better understanding a reference frame is defined, in which "longitudinal" or "z" means along the guide axis and "transverse" or "x" and "y" means perpendicular to it. As the guide forms a conservative potential for the transversely slow molecules, the velocity distribution for a hypothetical gas of state-selected molecules is the Boltzmann distribution for a thermal gas,

$$P(v_x) = \frac{1}{\alpha\sqrt{\pi}}\, e^{-v_x^2/\alpha^2} \quad (|v_x| < |v_{max}|)\,, \tag{1}$$

where v_{max} is the maximum transverse velocity. This velocity depends on the Stark shift and on the distance from the injection point to the axis.

Directly after injection in the guide, the longitudinal velocity distribution is the same as that of molecules in the reservoir passing through a plane from one side with velocity component v_z perpendicular to the plane:

$$P(v_z) = \frac{2v_z}{\alpha^2}\, e^{-v_z^2/\alpha^2}. \tag{2}$$

Longitudinal velocity filtering is achieved by bending the guide with a certain radius of curvature. If the molecule is too fast, the centrifugal force exceeds the Stark force and the molecule leaves the guide. For every Stark shift there exists a maximum guided longitudinal velocity v_{lmax}. Choosing a large radius of curvature results in modest filtering in longitudinal direction, whereas a small radius of the order of 1 cm is expected to select molecules with a maximum total velocity of 20 m/s which can be trapped in an electrostatic trap. Equation (2) exhibits a unique property of the guide: the probability density rises linearly for small longitudinal velocities, compared to standard molecular beams, which show a cubic dependence. This results from the fact that our guide selects on energy and not on angle, keeping those molecules which are lost in a standard molecular beam collimated with apertures. This is the key reason for the efficiency of our guide.

3 Guiding efficiency

In this section the guiding efficiency of the present set-up is calculated [26]. The guiding efficiency is different for every gas as it depends critically on the molecular Stark shifts. Here, we present the calculations for ND_3 and show how the guiding efficiency varies according to the source temperature. The results are later used for comparison with the experimental data.

3.1 The guided fraction

The output flux is one of the key parameters of the slow-molecule source. We now estimate the guided fraction of ND_3 molecules emerging from an effusive source. For simplicity, we assume that the transverse and longitudinal degrees of freedom do not mix, i.e., a particle injected with zero transverse velocity will come out of the guide with zero transverse velocity. This is valid as long as the radius of the bend's curvature is much larger than the transverse width of the guide. Most molecules enter the guide off-axis so that they already have a higher potential energy which reduces their exit velocity to $|v| < |v_{max}|$. This can be taken into account yielding a small correction which we neglect here for simplicity. In the following, we calculate a lower limit of the guided fraction assuming that the selection in z-direction is influenced by the transverse velocity and that the two transverse directions fully mix.

The longitudinal cut-off velocity, v_{lmax} can be found by equating the centripetal force given by the Stark force with the centrifugal force, yielding $v_{lmax}^2 = v_{max}^2\, R/2r$ for a guide with the radius of curvature R and the open inner radius r. The molecules escape in the transverse direction if their total transverse velocity, $v_\rho = \sqrt{v_x^2 + v_y^2}$, exceeds v_{max}. As the filtering depends on both longitudinal and transverse velocity, for each v_z there exists a critical transverse velocity $v_{\rho max} < v_{max}$ given by $v_{\rho max}^2 = v_{max}^2 - 2v_z^2 r/R$ above which the molecule will be lost. The guided fraction of transversely slow molecules as a function of the longitudinal velocity is found from equation (1) by integrating in cylindrical coordinates:

$$f_\rho(v_z)dv_z = \int_0^{v_{\rho max}(v_z)} 2\pi v_\rho \frac{1}{\alpha^2\pi}\, e^{-v_\rho^2/\alpha^2} dv_\rho dv_z = \left(1 - e^{-[v_{\rho max}(v_z)]^2/\alpha^2}\right) dv_z. \quad (3)$$

The total guided flux as a fraction of the input flux in this limit can be written as a function of v_{max} alone and is obtained by integrating this result over the v_z-distribution from equation (2):

$$f = \int_0^{v_{lmax}} \frac{2v_z}{\alpha^2} e^{-v_z^2/\alpha^2}\; f_\rho(v_z)\; dv_z \quad (4)$$

$$= \frac{2r\left(e^{-Rv_{max}^2/(2r\alpha^2)} - 1\right) + R\left(1 - e^{-v_{max}^2/\alpha^2}\right)}{R - 2r}. \quad (5)$$

The knowledge about the Stark shifts of the various molecular states is required to determine the transverse cut-off velocities $v_{\rho max}$.

3.2 Stark shift of ND_3

ND_3 is a symmetric top molecule which has a pyramidal structure with the N atom at the top and the three D atoms at the base. Due to this structure the moments of inertia along the two principal axes perpendicular to the symmetry axis are equal and the rotational constant for these axes is $B = 5.14\ \mathrm{cm}^{-1}$, whereas the rotational constant for the symmetry axis is $C = 3.15\ \mathrm{cm}^{-1}$ [27]. The rotational energy levels (in units of cm^{-1}) can be calculated from:

$$W_{\mathrm{rot}} = BJ(J+1) + (C-B)K^2 \quad (6)$$

where J is the rotational quantum number and K is the projection of J on the molecule's symmetry axis. One of the normal vibrational modes of ND_3 is the mode where the N atom vibrates back and forth towards the plane of the three D atoms which is also called the umbrella mode. The system can be described by a double-well potential and the nitrogen atom can tunnel through the base of the molecular pyramid, inverting the molecular structure. The tunnelling through the barrier is responsible for a splitting between the two inversion levels which amounts to $W_{\mathrm{inv}} = 0.053\ \mathrm{cm}^{-1}$ for the vibrational ground state of ND_3. Higher vibrational states are not populated at room temperature. This comparatively small splitting has a strong effect on the Stark shift of the molecule. In electric fields which are relevant to our experiment, 0−100 kV/cm, the Stark shift can be approximated by [28]:

$$\Delta W_{\mathrm{Stark}} = \pm\sqrt{\left(\frac{W_{\mathrm{inv}}}{2}\right)^2 + \left(\mu\,|\boldsymbol{E}|\,\frac{MK}{J(J+1)}\right)^2}, \quad (7)$$

where μ denotes the dipole moment ($\mu = 1.47$ D) and M is the projection of J on the electric field $\boldsymbol{E}$. Due to the small splitting, W_{inv}, about 76% of the molecular states in a thermal ensemble show a Stark shift which deviates less than $0.005\ \mathrm{cm}^{-1}$ from the linear behavior at electric fields $E > 10$ kV/cm. This is predominantly the case for states where J, $|K|$, and $|M|$ are roughly equal which results in a comparatively high Stark shift. For this estimate we took into account that the inversion splitting depends on the particular quantum numbers J and K according to an approximate equation for the inversion splitting from [29]. Note that the states which show a linear Stark shift are most likely to be guided so that the guided molecules have linear Stark shifts to a very good approximation. Compared to ND_3, the inversion splitting of NH_3 is much higher ($W_{\mathrm{inv}} = 0.79\ \mathrm{cm}^{-1}$) which results in weaker and more quadratic Stark shifts.

At room temperature, states with rotational quantum number up to $J = 25$ occupy more than 99.99% of the population. The Stark shifts of these molecular states were calculated and similar Stark shifts are grouped together. Figure 2 shows the relative occurrence of these Stark shifts at electric field strength of 100 kV/cm in a thermal gas at $T = 300$ K. With equation (5) and the Stark shift distribution the guided fraction of the lfs molecules can be calculated to be 4.0×10^{-5} for $T = 300$ K and 1.5×10^{-4} for $T = 150$ K with $R = 12.5$ mm and $r = 1.2$ mm. We find that the relative abundance of the Stark shifts does not change significantly when decreasing the temperature down to $T = 150$ K. From these numbers we predict that it should be possible to increase the flux by a factor of approximately 3.75 by cooling down the nozzle. The internal state distribution of the guided molecules is peculiar,

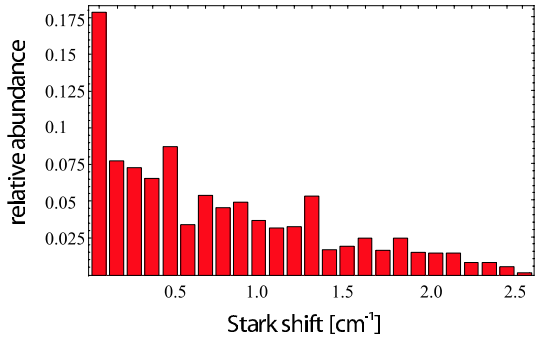

Fig. 2. Histogram of the Stark shift occurrence at a field strength of 100 kV/cm in a thermal gas of ND_3 at $T = 300$ K. Similar shifts are gathered in small groups which cover a range of 0.093 cm^{-1}.

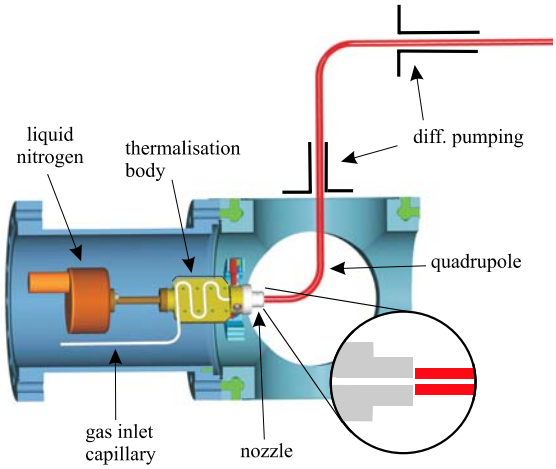

Fig. 3. Cut through the gas inlet chamber of the experimental set-up. The liquid nitrogen cooling stage with the connected gas inlet system and the quadrupole is shown. Gas enters the chamber in a thin flexible Teflon tube which passes through a copper block before it ends in the exit nozzle. The copper block with the nozzle assembly is connected to the liquid nitrogen reservoir via a thermal link and heating elements allow nozzle temperature variations from 100 K to 400 K. The nozzle assembly highlighted in the inset is aligned to the quadrupole axis. Between the quadrupole electrodes and the ceramic source assembly there is a gap of 0.5 mm.

as it is enriched by states with a large Stark shift, i.e. those states with a large value of $|MK/(J(J+1))|$.

4 The experimental set-up

The experimental set-up shown in Figure 3 consists of a cooled nozzle assembly and the electrostatic quadrupole. Gas can be let in from a reservoir at room temperature which is connected to the nozzle via a long Teflon capillary. The nozzle is mounted on a heatable copper block which is connected via a thermal link to a liquid nitrogen reservoir. This allows nozzle temperature variation between 100 K and 400 K. In order to effectively cool the gas, it is guided along a winding path of ≈8 cm length in a thin flexible

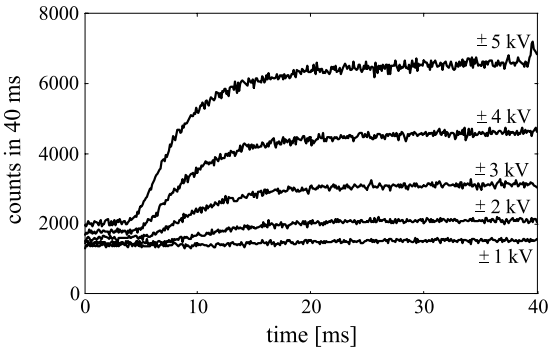

Fig. 4. Detector signal as a function of the on-time of the quadrupole. The signal amplitude increases with the applied electrode voltages and for higher voltages the signal rises earlier.

Teflon capillary (ø = 1.5 mm inner diameter) inside the copper block before it flows through the nozzle with an inner diameter of 1.5 mm. To minimize the thermal contact, the nozzle assembly is held by three glass balls which are embedded in a metal ring. Between the quadrupole electrodes and the nozzle a gap of 0.5 mm exists to avoid heat transfer. The quadrupole is formed by 50 cm long and 2 mm diameter stainless steel electrodes, with a 1 mm gap between neighboring electrodes. The radius of curvature of the first bend is 12.5 mm and further downstream there is a second bend with a radius of curvature of 25.0 mm. Only in early measurements which will be shown in section 5.1 the radii were both 25.0 mm. Every bend section is followed by a narrow tube of ≈8 cm length for differential pumping. Most of the injected molecules are not guided and escape into the first vacuum chamber, where an operational pressure of a few times 10^{-7} mbar is maintained by a 500 l/s turbo molecular pump. In the detection chamber, where a pressure below 10^{-10} mbar is achieved by using a 100 l/s ion pump, the guided molecules are detected with an efficiency of about 10^{-4} counts/molecule by a quadrupole mass spectrometer (QMS) [Hiden Analytical, HAL 301/3F]. The QMS is operated in pulse-counting mode and the pulses are recorded with a multi-channel scaler. For detecting ND_3 the QMS is set on mass 20, the mass of ND_3.

5 Filtering and guiding ND_3

5.1 Signal amplitude analysis

Here we present the guiding signal as a function of the applied quadrupole voltage. For this measurement we periodically apply voltages between ±1 kV to ±5 kV on the quadrupole which results in a maximum field strength of ≈90 kV/cm between the electrodes at ±5 kV. As soon as the field is switched on, the slow molecules are kept within the guide. For the highest voltage it takes about 4 ms till the fastest molecules arrive at the detector. Figure 4 shows the time-of-flight signals for the different voltages obtained after 400 switching cycles. Note that the delay in

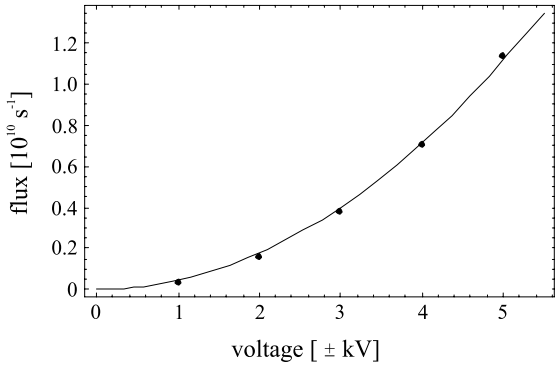

Fig. 5. The quadratic dependence of the guided flux as a function of the applied electrode voltages. The line is a quadratic fit to the data.

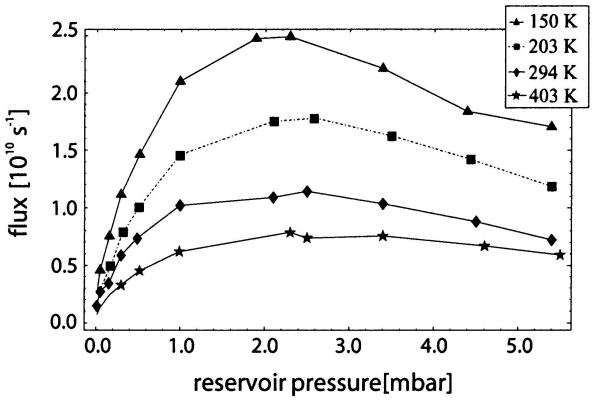

Fig. 6. Flux dependence on the reservoir pressure at different nozzle temperatures. For lower temperatures the guiding efficiency is increased as long as the gas has a vapor pressure higher than the local nozzle pressure.

the signal rise increases as the voltage on the quadrupole is reduced, because the maximum guidable velocity decreases for smaller voltages. It can be seen that the background level of the signal traces grows with the quadrupole voltages. This is due to the different average background pressure in the detection chamber for a measurement at a particular field strength. The average background pressure depends on the guided flux which is caused by the switching and it increases when the quadrupole voltages are increased.

The signal amplitude shows a quadratic dependence on the applied electric field, as can be seen from Figure 5. This is expected because under the assumption that the molecules show a linear Stark effect and that the longitudinal (v_l) as well as the transverse (v_ρ) velocities are much smaller than the mean thermal velocity inside the reservoir, the flux Φ in the guide is:

$$\Phi \propto \int_{v_\rho=0}^{v_{\rho max}} 2\pi v_t \, \mathrm{d}v_t \int_{v_l=0}^{v_{l max}} v_l \mathrm{d}v_l \propto {v_{\rho max}}^2 {v_{l max}}^2 \propto E^2, \tag{8}$$

where E is the depth-determining electric field strength. Equation (8) is valid for every molecule with a linear Stark shift, and therefore also for an ensemble of molecules with different, but linear, Stark shifts.

5.2 Flux calibration

In order to calibrate the flux of the guided molecules, the sensitivity of the QMS for ND_3 is estimated under the present experimental conditions. To this end, a constant flow of ND_3 into the system is maintained and, when a certain partial pressure of ND_3 has been established in the detection chamber, a mass spectrum is taken. The peaks with the strongest contribution in the mass spectrum are corrected according to their different electron ionization probability with the particular gas correction factor [30] and from the corrected mass spectrum the relative abundance of ND_3 in the residual gas can be determined. By measuring the pressure with an ionization gauge, the total particle density can be estimated and, as the relative abundance is known, the absolute number of ND_3 molecules in the ionization volume can be determined. Our estimate results in a QMS sensitivity within a factor of two from the $\approx 10^{-4}$ counts/molecules estimate which is provided by the manufacturer, for room-temperature molecules. An accurate flux estimation also requires a solid angle correction as the guided molecules are spatially filtered by an inlet aperture (ø = 5 mm) on the QMS ionization unit. From the angle distribution measurement of the exit beam shown in Section 7 we have derived that a fraction of 10 percent of the guided flux reaches the detector. These corrections are employed for the flux estimation.

5.3 Flux at different nozzle pressures and temperatures

The measurements were performed in a reservoir pressure range from 0.05 mbar to 5.5 mbar and the nozzle temperature has been varied between 100 K and 400 K. Some of the resulting flux curves are shown in Figure 6. Let us first discuss the room-temperature curve at 294 K. For low pressures the flux increases linearly in pressure and it starts deviating from the linear dependence above a reservoir pressure of ≈0.3 mbar. This leads to a pressure inside the nozzle which lies between the Knudsen regime, where the mean free path is larger than the nozzle diameter and the viscous regime, where intermolecular collisions along the capillary frequently occur. When the reservoir pressure is further increased the guided flux reaches a maximum at 2.5 mbar. In consideration of the gas inlet stage conductance we calculate that at this reservoir pressure the average pressure in the last 10 mm of the nozzle is close to 0.1 mbar. At this value the mean-free path of the molecules is of the order of the nozzle diameter and collisions play an important role. When the pressure is further increased, collisions quickly remove the slow molecules and the guided flux decreases again.

As the guiding technique allows filtering of the slowest molecules from a thermal gas, its natural extension is that the filtering efficiency can be increased if the average velocity of the thermal gas is reduced, i.e., if the effusive

source itself is cooled. From our approximate analytical theory from Section 3.2 we know that we can expect an increase in guiding efficiency by a factor of ≈3.75 when we substitute $T = 150$ K in our model instead of $T = 300$ K. The guided flux is the product of the input from the nozzle and the guided fraction, f. For an ideal gas it is expected that the particle flux through the nozzle at a pressure p and temperature T is proportional to $p/\sqrt{T}$. In order to see how this affects the gas input we calculated the pressure in the nozzle. For our geometry and the pressure drop over the whole inlet stage we estimate the conductance with standard textbook expressions [31] and calculate the flow rate through the system. The flow rate allows us to calculate the local pressure at every point along the inlet capillary. The pressure is expected to drop linearly along the warm and the cold sections of the capillary. At 150 K the pressure in the cold section is about 10% lower compared to the pressure at 300 K. The variations in pressure and temperature contributions compensate each other to some extend so that the flux through the nozzle is expected to increase by a factor of $0.9/\sqrt{1/2}$ according to the $p/\sqrt{T}$-dependence when the temperature is reduced from 300 K to 150 K. If this factor is multiplied with the increase in guiding efficiency, the guided flux is expected to increase by a factor of ≈4.8 in the case of an ideal gas.

It can be seen in Figure 6 that decreasing the temperature leads to an increase in the guided flux and the maximum flux changes in good approximation by a factor of two when the temperature is reduced from 300 K to 150 K. As our model is only valid in the regime where the guided flux rises linearly with the reservoir pressure, we compare the rising slopes of the two flux curves. The slope of the flux curve for 150 K rises only twice as fast as the room-temperature curve. This deviation from the model might be explained by the fact that 150 K is below the triple point of ND_3 at 195 K and the molecules begin to stick to the capillary walls which increases the impedance of the gas inlet capillary. As we have no access to the pressure inside the nozzle, this is difficult to verify. However, the hypothesis is supported by the different pressure rises in the first filtering chamber when injecting gas at different temperatures: at $T = 150$ K the pressure rise is half that at $T = 300$ K for a comparable reservoir pressure, hinting to a smaller gas input at lower temperatures. The exact value and position of the maximum in the flux curve is not yet understood, but will depend on the flow dynamics of fast and slow molecules in the nozzle in the intermediate pressure regime between Knudsen and viscous flow. Also because of the lacking accurate nozzle pressures, this seems very difficult to model. Nevertheless, it is striking that the maximum flux in the curves occurs in the same reservoir pressure range.

We expect ≈130 K as a lower temperature limit for a measurable guiding signal, because then the saturated vapor pressure of ammonia [32] is less than the local nozzle pressure at usual reservoir pressures and it decreases exponentially with temperature. This leads to a rapid condensing of the gas at the nozzle walls and for lower temperatures the guiding signal should fall off rapidly. Figure 7 shows the maximum flux as a function of the nozzle temperature for temperatures down to 100 K. As expected the flux vanishes for temperatures below 130 K. The range between 150 and 400 K is well fitted by a T^{-1} dependence, which is not yet understood.

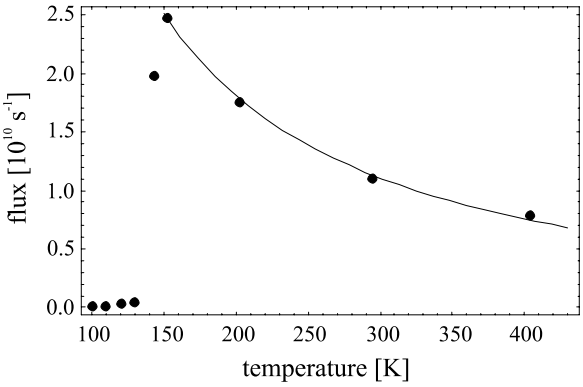

Fig. 7. Maximum flux at different nozzle temperatures. At 150 K the flux reaches a maximum and it decreases for lower temperatures as the vapor pressure of ND_3 for $T < 130$ K is less than the local nozzle pressure. The black curve indicates a T^{-1} dependence for temperatures above 150 K.

5.4 Buffer-gas attempts

In an attempt to extend the reservoir cooling technique to temperatures below 150 K we mixed ND_3 with argon and injected this mixture through the nozzle which was cooled to a temperature of 140 K. Noble gases like argon still have a considerable vapor pressure below 150 K and the idea was that they can be used as a buffer gas which enables thermalization of the ND_3 molecules to the nozzle temperature by collisions with the buffer gas, but avoiding wall collisions of the ND_3 molecules. The non-polar noble gases are hfs and will not be guided. For this idea to work, the partial pressure of the buffer gas has to exceed that of ND_3 by far, in order for the mean free path of the molecules to be smaller than the nozzle diameter so that the ND_3 is prevented from sticking to the walls. Of course, this then automatically leads to a speed-up of the average output velocity by collisions, similar to the transition from a effusive source to a supersonic nozzle. A priori it was not clear which effect wins: the gain in signal because the cold molecules do not freeze out on the walls, or the loss in signal because slow molecules are removed from the nozzle and the guide by collisions with the fast buffer gas.

Figure 8 shows the flux as a function of the reservoir pressure when ND_3 is injected together with argon as buffer gas. The partial pressure of ND_3 is held constant at 0.5 mbar and the pressure rise up to 5.0 mbar is caused by the argon. Clearly, the flux decreases when a buffer gas is added. We conclude that buffer gas addition at the temperatures just below the standard operation regime of our apparatus is not very promising.

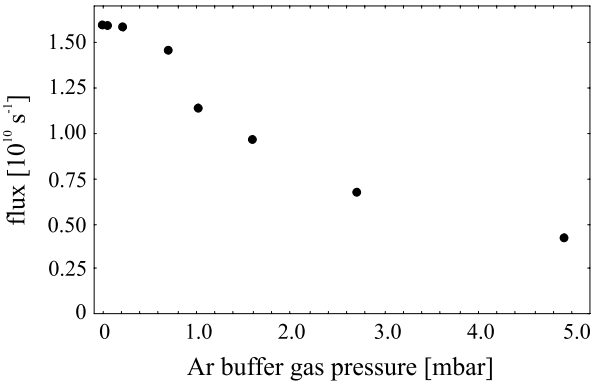

Fig. 8. The flux as a function of the partial pressure of the argon buffer gas that is admixed to the ND_3 gas in the reservoir. The nozzle temperature is 140 K. Clearly, the buffer gas is detrimental to the guided slow molecule flux.

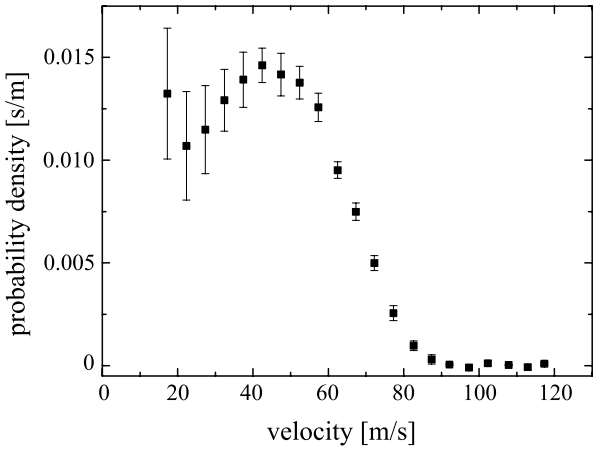

Fig. 9. Velocity distribution of the guided ND_3 molecules derived from data obtained with electrode voltages of ±5 kV at a nozzle temperature of 140 K. The data below 20 m/s are affected with large systematic errors. The maximum of the probability density is at 40 m/s which corresponds to a one-dimensional (translational) temperature of ≈4 K. The error bars in the graph denote statistical errors.

6 Velocity distribution

The velocity distribution of the guided molecules provides essential information about their (external) temperature and it reveals basic properties of the molecular beam. With the delay and the rising slope of a time-of-flight signal the longitudinal velocity distribution can be derived by differentiation. For an accurate calculation of the velocity distribution one has to take into account several features of the interplay between guide and detector: (1) when the molecules leave the guide they are accelerated towards the detector by the fringe field. The probability that the molecules enter the ionization volume of the QMS varies for different velocities, because the longitudinally slow molecules are more likely to miss this volume as they spread over a larger solid angle. (2) The ionization probability is velocity dependent because compared to the fast molecules, the slow molecules spend more time in the ionization volume and so their ionization probability is higher. The effect described in (1) results in an underrepresentation of the slow molecules in the measured signal. A correction for this effect can be extracted from a Monte Carlo simulation which provides information about the fraction of molecules from different velocity classes hitting the detector. The effect described in (2) leads to an overrepresentation of the slow molecules compared to the fast ones which means that it compensates to some extend the effect (1). In order to calculate the accurate velocity distribution the measured signal has to be corrected for these effects. Especially for velocities below 20 m/s these corrections play a significant role. In [8] a velocity distribution with all corrections included has been calculated for formaldehyde where another guide geometry has been used. It shows the linear increase of the probability density for small velocities which is a characteristic feature of our guiding technique. Figure 9 shows the velocity distribution of guided ND_3 molecules obtained from uncorrected data. The part of the experimental data which provides information about velocities below 20 m/s is affected by uncertainties as the time-of-flight signal shows a small but permanent rise for later arrival times. This rise is not only caused by slow molecules because an additional local pressure increase near the detector originating from the guided molecules might play a role. Below 20 m/s this effect is much stronger than the effects resulting from the corrections and therefore the data is affected with large systematic errors. The velocity distribution shows a maximum near 40 m/s which corresponds to a temperature of ≈4 K. Note that for a single molecular state the velocity distribution should show a relatively sharp cut-off. As our gas consists of a mixture of states with different Stark shifts the cut-off is smeared out and it can be seen from [8] that the velocity distribution can be described by a 1-dimensional thermal distribution.

7 The exit beam

In order to characterize the angular distribution of the exit beam the flux density has been measured in a plane perpendicular to the guide along two orthogonal axes x and y through the center of the guide. For this measurement the QMS has been translated with a vacuum manipulation stage along the two axes. The flux dependence is shown in Figure 10a. It can be seen that the beam profile is slightly asymmetric which can be caused by the fact that the electrodes do not have exactly the same length. The FWHM of the distributions is approximately 1 cm at a distance of 18 mm behind the exit. In the next measurement the QMS is positioned in the center of the beam and the distance between the guide and the QMS is varied. For every position the flux is recorded (see Fig. 10b) and as expected the flux decreases according to a $1/z^2$-dependence with the distance. In Figure 10c the beam profile along the y-axis has been measured with different electrode voltages of ±3 kV and ±5 kV at a distance of 18 mm between the guide and the center of the QMS ionization unit. For both

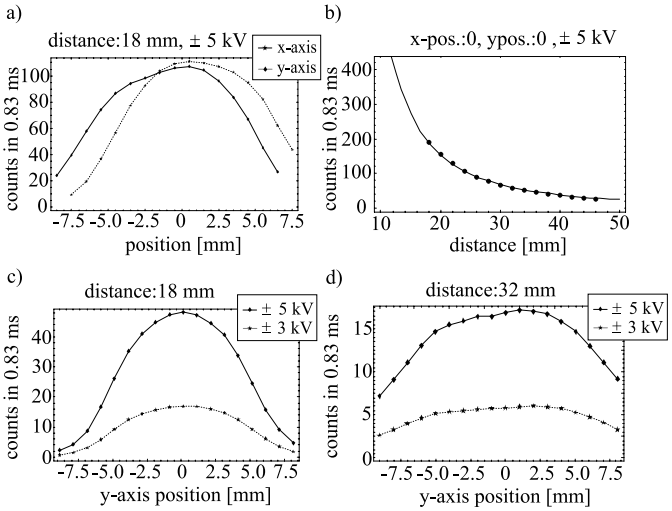

Fig. 10. (a) Angle distribution of the guided flux along two perpendicular axes at a distance of 18 mm between the center of the QMS ionization unit and the end of the guide. The slight asymmetry can be explained by small electrode length variations. The electrode voltages are ±5 kV. (b) Flux as a function of the distance between the guide and the center of the QMS ionization unit at electrode voltages of ±5 kV. The line is an inverse quadratic fit to the data. (c) Angle distribution of the guided flux along one axis with two different electrode voltages ±3 kV and ±5 kV. The angle distribution remains unchanged as the lower curve is proportional to the upper curve. The same is valid for the measurement in (d) where the distance has been increased to 32 mm. Note that the pressure conditions for the different measurements were not the same.

measurements the angle distribution is the same but for an overall scale factor. The same measurement has been repeated for a larger distance of 32 mm and the data is displayed in Figure 10d.

8 Conclusion and outlook

We provided a detailed overview of theoretical and experimental aspects of filtering slow ND_3 molecules emerging from an effusive source with a bent electrostatic quadrupole guide. The dependence of the filtering efficiency on the source parameters temperature and pressure was investigated and we measured the flux of the guided molecules as a function of the applied electric fields. We have successfully demonstrated that a flux of ND_3 of the order of 2×10^{10}/s can be achieved with the presented technique which is in principle applicable to any molecule with a reasonably high Stark shift. In this paper the experiments were done with ND_3 which shows a predominantly linear Stark shift but we also performed experiments with H_2CO yielding similar results. In principle the guiding technique is applicable as long as the molecules have a sufficiently high Stark shift to mass ratio. Reference [33] contains a list of polar diatomic and polyatomic molecules with their relevant properties which are suited for electric trapping experiments. Furthermore the longitudinal velocity distribution has been measured with a time-of-flight measurement and the velocity distribution of the guided molecules shows a maximum around 40 m/s. These results show that the filtering technique is able to provide a high flux of slow molecules which in principle can be trapped in the field minimum of an electrostatic trap [34]. Even though the molecules are still hot internally, which results in a high number of internal states populated, the slow beam as it stands already offers new perspectives for experiments in interferometry and cold chemistry. Here we have focused on the filtering of molecules in low-field seeking states with electrostatic fields. High-field seekers, as for instance the ground state of any molecule, cannot be manipulated by the use of electrostatic fields. In order to extend this technique to both high- and low-field seekers the present set-up can be used to guide both species in alternating electric fields. As a first step in this direction we recently demonstrated that molecules can be guided in a quadrupole driven with an alternating potential [35].

We acknowledge financial support by the DFG under SPP 1116.

References

1. J.J. Hudson, B.E. Sauer, M.R. Tarbutt, E.A. Hinds, Phys. Rev. Lett. **89**, 023003 (2002)
2. B. Brezger, L. Hackermüller, S. Uttenthaler, J. Petschinka, M. Arndt, A. Zeilinger, Phys. Rev. Lett. **88**, 100404 (2002)
3. N. Balakrishnan, A. Dalgarno, Chem. Phys. Lett. **341**, 652 (2001)
4. J.D. Weinstein, R. de Carvalho, T. Guillet, B. Friedrich, J.M. Doyle, Nature **395**, 148 (1998)
5. H.L. Bethlem, G. Berden, G. Meijer, Phys. Rev. Lett. **83**, 1558 (1999); H.L. Bethlem, F.M.H. Crompvoets, R.T. Jongma, S.Y.T. van de Meerakker, G. Meijer, Phys. Rev. A **65**, 053416 (2002)
6. M.R. Tarbutt, H.L. Bethlem, J.J. Hudson, V.L. Ryabov, V.A. Ryzhov, B.E. Sauer, G. Meijer, E.A. Hinds, Phys. Rev. Lett. **92**, 173002 (2004)
7. J.R. Bochinski, E.R. Hudson, H.J. Lewandowski, G. Meijer, Jun Ye, Phys. Rev. Lett. **91**, 243001 (2003)
8. S.A. Rangwala, T. Junglen, T. Rieger, P.W.H. Pinkse, G. Rempe, Phys. Rev. A **67**, 043406 (2003)
9. A. Fioretti, D. Comparat, A. Crubellier, O. Dulieu, F. Masnou-Seeuws, P. Pillet, Phys. Rev. Lett. **80**, 4402 (1998)
10. T. Takekoshi, B.M. Patterson, R.J. Knize, Phys. Rev. Lett. **81**, 5105 (1998)
11. A.N. Nikolov, E.E. Eyler, X. Wang, H. Wang, J. Li, W.C. Stwalley, P.L. Gould, Phys. Rev. Lett. **82**, 703 (1999)
12. C. Gabbanini, A. Fioretti, A. Lucchesini, S. Gozzini, M. Mazzoni, Phys. Rev. Lett. **84**, 2814 (2000)
13. R. Wynar, R.S. Freeland, D.J. Han, C. Ryu, D.J. Heinzen, Science **287**, 1016 (2000)
14. U. Schlöder, C. Silber, C. Zimmermann, Appl. Phys. B. **73**, 801 (2001)
15. E.A. Donley, N.R. Claussen, S.T. Thomson, C.E. Wieman, Nature **417**, 529 (2002)
16. C.A. Regal, C. Ticknor, J.L. Bohn, D.S. Jin, Nature **424**, 47 (2003)
17. J. Herbig, T. Kraemer, M. Mark, T. Weber, C. Chin, H.C. Nägerl, R. Grimm, Science **301**, 1510 (2003)

18. S. Dürr, T. Volz, A. Marte, G. Rempe, Phys. Rev. Lett. **92**, 020406 (2004)
19. K.E. Strecker, G.B. Partridge, R.G. Hulet, Phys. Rev. Lett. **91**, 080406 (2003)
20. J. Cubizolles, T. Bourdel, S.J.J.M.F. Kokkelmans, G.V. Shlyapnikov, C. Salomon, Phys. Rev. Lett. **91**, 240401 (2003)
21. S. Jochim, M. Bartenstein, A. Altmeyer, G. Hendl, C. Chin, J. Hecker Denschlag, R. Grimm, Phys. Rev. Lett. **91**, 240402 (2003)
22. K. Xu, T. Mukaiyama, J.R. Abo-Shaeer, J.K. Chin, D.E. Miller, W. Ketterle, Phys. Rev. Lett. **91**, 210402 (2003)
23. M. Gupta, D. Herschbach, J. Phys. Chem. A **105**, 1626 (2001)
24. M.S. Elioff, J.J. Valentini, D.W. Chandler, Science **302**, 1940 (2003)
25. B. Ghaffari, J.M. Gerton, W.I. McAlexander, K.E. Strecker, D.M. Homan, R.G. Hulet, Phys. Rev. A **60**, 3878 (1999)
26. P.W.H. Pinkse, T. Junglen, T. Rieger, S.A. Rangwala, G. Rempe, *Interactions in Ultracold Gases*, 477, edited by M. Weidemüller, C. Zimmermann (Wiley-VCH, Weinheim, 2003)
27. G. Herzberg, *Infrared and Raman Spectra of Polyatomic Molecules* (van Nostrand Reinhold, Inc., New York, 1945)
28. C.H. Townes, A.L. Schawlow, *Microwave Spectroscopy* (Dover Publications, Inc., New York, 1975)
29. R.G. Nuckolls, L.J. Rueger, H. Lyons, Phys. Rev. **89**, 1101 (1953)
30. R.L. Summers, NASA Technical Report, NASA-TN-D-5285 (1969)
31. M. Wutz, H. Adam, W. Walcher, K. Jousten, *Handbuch Vakuumtechnik, 7. Auflage* (Vieweg, Braunschweig/Wiesbaden, 2000)
32. CRC Handbook of Chemistry and Physics, 74. Edition 1993-1994, **6**-94
33. H.L. Bethlem, F.M.H. Crompvoets, R.T. Jongma, Y.T. van de Meerakker, G. Meijer, Phys. Rev. A **65**, 053416 (2002)
34. H.L. Bethlem, G. Berden, F.M.H. Crompvoets, R.T. Jongma, A.J.A. van Roij, G. Meijer, Nature **406**, 491 (2000); F.M.H. Crompvoets, H.L. Bethlem, R.T. Jongma, G. Meijer, Nature **411**, 174 (2001)
35. T. Junglen, T. Rieger, S.A. Rangwala, P.W.H. Pinkse, G. Rempe, Phys. Rev. Lett. **92**, 223001 (2004)